On the interference arising from random spatial fields of interferers utilizing multiple subcarriers

Zheng *et al. J Wireless Com Network* (2022) 2022:27
https://doi.org/10.1186/s13638-022-02110-w

EURASIP Journal on Wireless Communications and Networking

RESEARCH Open Access

On the interference arising from random spatial fields of interferers utilizing multiple subcarriers

Ce Zheng[1], Malcolm Egan[2*], Laurent Clavier[1], Gareth W. Peters[3] and Jean-Marie Gorce[2]

*Correspondence:
malcom.egan@inria.fr
[2] CITI Laboratory, Univ Lyon, INSA Lyon, Inria, Villeurbanne, France
Full list of author information is available at the end of the article

Abstract

Effective symbol detection, channel estimation and decoding of channel codes require an accurate characterization of the noise probability distribution. In many systems, notably the internet of things, noise is largely in the form of interference, arising from a massive number of simultaneous transmissions from uncoordinated devices. Obtaining the probability distribution of the interference is a challenging problem due to the use of non-orthogonal multiple access schemes over several subcarriers (leading to multivariate statistical models) and the heavy-tailed nature of the interference due to the random locations of devices. In this paper, we derive a novel tractable characterization of the interference probability distribution based on an application of Sklar's theorem to develop a combination of α-stable and t-copula dependence models. We demonstrate that this formulation produces an accurate statistical modeling framework that admits efficient parameter estimation methods. As an illustration of the utility of our models, we develop a simple-to-implement nonlinear receiver when a binary signal is transmitted over all subcarriers by the desired transmitter, which is effective in a range of scenarios and can significantly outperform existing approaches.

Keywords: Multivariate interference, Heavy-tailed distributions, Stochastic geometry

1 Introduction

With the increasing scale of wireless network deployments for the internet of things (IoT), an ongoing question is how to ensure that these networks meet reliability and latency requirements. A difficulty in network design is that interference from a large number of devices, even if they operate at low power levels, can significantly degrade the performance of other nearby wireless communication networks.

A key reason for such performance degradation is the uncoordinated nature of devices, which typically requires interference to be treated as noise. The lack of coordination arises both in where devices are located and when they transmit. As a consequence, point process models for device locations have played an important role in characterizing the interference. A number of different models have been introduced in wireless communications, both in the IoT and cellular settings. These include

homogeneous Poisson point processes [1–5], cluster [6], hard-core [7], nonhomogeneous Poisson [8] and determinantal [9] processes.

However, this existing work has largely focused on network-level criteria such as outage and coverage probabilities. On the other hand, another critical issue is the design of detection and coding schemes, which rely on a good characterization of the noise and interference probability distributions for the amplitude and phase, rather than just for the instantaneous received power. This issue of the interference probability distribution arising from devices located according to point processes has been addressed only for narrowband transmissions with a single carrier.

Due to the widespread use of OFDM in IoT systems, such as in NB-IoT [10], an important question is how to characterize the interference amplitude and phase distribution when multiple subcarriers are utilized. In particular, the interference is multivariate, forming a random vector arising from the signals observed on each subcarrier. This introduces new questions as devices may access multiple subcarriers simultaneously, leading to non-trivial statistical dependence between the interference on different subcarriers. As for the case of narrowband transmissions using a single carrier, addressing this question is important to improve the design of symbol detection rules and channel coding schemes.

In this paper, we characterize the interference amplitude and phase statistics arising from spatial point processes where uncoordinated interferers randomly select the subcarriers they utilize. We consider homogeneous Poisson point processes (HPPPs) and certain families of Poisson cluster and Matérn hard-core type II processes, which are able to model attraction and repulsion useful to account for physical considerations (e.g., the presence of roads or buildings) or protocols such as CSMA [7]. Models incorporating random selections of subcarriers are well suited to wireless networks for the Internet of Things (IoT) exploiting the NB-IoT protocol [11], where interference must be treated as noise by the intended receiver; that is, advanced multiuser detection methods are not available due to the absence of pilot symbols. In particular, since Release 13 of the 3GPP LTE standard [10], NB-IoT allows each device to transmit on up to 12 subcarriers in the NPUSCH [10]. As these subcarriers are selected randomly by each device, the signal observed by a desired receiver exhibits complex statistical dependence between each subcarrier. The scenario is also relevant when a large-scale network exploiting SCMA with coding in both time and frequency [12].

In realistic models of interfering networks, the location and fading associated with each interferer are not known by the desired receiver. As a consequence, there is an increase in the uncertainty of the received signal. Theoretical (see, e.g., [13–16]) and recent experimental [17–19] evidence strongly suggests that the resulting interference should therefore be modeled by heavy-tailed distributions; that is, the probability of large interference is much higher than predictions from Gaussian models would suggest.

With an accurate interference model in hand, it is then feasible to improve receiver design. For example, symbol detection relies on knowledge of the interference statistics through tests based on the likelihood ratio of the received signal given each possible transmitted symbol [20, 21]. Accurate interference models are also necessary for channel estimation and decoding of channel codes [22].

1.1 Related work

Since the initial work on interference arising from Poisson point process models, it has been known that the in-phase or quadrature baseband interference signal on a *single* subcarrier has α-stable statistics, assuming an infinite network and zero guard-zone radii [13–16]. For finite networks and non-zero guard-zone radii, the Middleton distribution arises [6]. It has also been shown that, again for a single subcarrier, the interference from a Poisson-Poisson cluster process also admits Middleton interference statistics [6]. There has been further work establishing that Poisson point processes can well approximate a range of other point process models (e.g. via Ripley's K-function [23] or the mean interference [24, 25]). The dependence over time of the interference has also been studied in [26], which characterizes the first and second moments in Matérn point processes with Matérn thinning, and in [27], which characterizes the joint distribution of the interference over time in HPPPs.

A key property of α-stable or Middleton statistics is their heavy-tailed nature, where for instance α-stable models have infinite variance (except when $\alpha = 2$) and may exhibit infinite mean depending on the tail index $\alpha \in (0, 2)$. While no real system will admit received signals with infinite variance (due to the presence of guard zones or near field propagation), α-stable models capture the slow decay of the tails for the interference probability density function arising in real measurements [17–19]. Due to the fact that α-stable models enjoy well-studied parameterizations and relative tractability, they are often preferred to other heavy-tailed models and provide superior modeling capability when compared to classical Gaussian models when heavy tails are present. Evidence for this tractability is apparent in existing work, which derives useful expressions for the probability of error [15], optimal linear combining strategies [20, 21], power control [28], channel capacity [29] and optimal input distributions [30].

Nevertheless, the interference statistics for wireless networks exploiting multiple subcarriers in the uplink have not been characterized. This contrasts with the large body of work focusing on network-level metrics, particularly for cellular systems (see, e.g., [1]). The difficulty in analyzing the interference statistics—which are now multivariate due to the presence of multiple subcarriers—arises due to the complex statistical dependence between the interference on each subcarrier.

On the other hand, multivariate statistical models with α-stable marginals[1] (i.e., α-stable interference on each subcarrier) have been treated in general within the statistics literature [31]. A key tool is the notion of a copula, which has also been sparingly used in signal processing (see, e.g., [32, 33]); albeit not in the context of interference modeling with the exception of [34, 35], which did not consider a specific source of interference and focused on the general impact of nonlinear dependence (i.e., beyond correlation) via numerical simulation. However, it is not straightforward to directly apply copula techniques to interference modeling. Indeed, a specific copula model must be selected in order to ensure an adequate tradeoff between accuracy and tractability. In particular, sufficiently low-complexity parameter estimation techniques are required.

[1] We note that a multivariate model with α-stable marginals is not necessarily a multivariate α-stable model, as discussed in the sequel.

1.2 Main contributions

A full characterization of the interference statistics has two components: (i) an analytically tractable statistical model; and (ii) low-complexity algorithms in order to perform parameter estimation. With such a characterization, detection algorithms with improved performance can then be developed.

In this paper, we address these challenges and make the following main contributions[2]:

1. When interferers randomly select a subset of subcarriers, motivated by NB-IoT networks, we rigorously establish convergence in distribution of interference induced by families of Poisson cluster processes and Matérn hard-core type II processes—defined precisely in Sect. 3—to interference induced by a HPPP. This provides a unifying framework to analyze interference from certain general families of point processes via HPPP.
2. For interferer locations governed by HPPP, we derive exact statistics for the multivariate interference arising from multiple subcarriers when all devices transmit on the same subcarriers. When devices randomly select the subcarriers that they use, we propose a model consisting of α-stable marginals and a t-copula function (a specific family of copula models) to capture the heavy-tailed nature of the interference and dependence between distinct subcarriers.
3. Exploiting the structure of the interference, we derive a low-complexity estimator for the multivariate interference model parameters. We show via simulations that the performance of our low-complexity estimator is in good agreement with the standard maximum likelihood estimator for general multivariate models described by t-copula function and α-stable marginals.
4. Via Monte Carlo simulations, we verify that our model is a good approximation in terms of the Kullback-Leibler divergence (KL divergence) for the true statistics of the interference. This is true even for non-Poisson point processes that arise from realistic network parameters.
5. To verify the utility of our model, we study the probability of error for binary detection in the presence of multivariate interference arising from a Poisson spatial field of interferers. We show that by exploiting our model, the probability of error can be significantly reduced compared with existing approaches in the literature, which either assume Gaussian models, or independent α-stable interference on each subcarrier well as in-phase and quadrature components.

The remainder of this paper is organized as follows: Sect. 2 describes the system model. Section 3 characterizes the multivariate impulsive interference when interferers are located according to a HPPP, a doubly Poisson cluster process or a Matérn hard-core process of type II. Section 4 proposes a low-complexity parameter estimation method tailored to the interference model. Section 5 verifies the models and the proposed estimation method. Section 6 studies the impact of multivariate impulsive interference on receiver design. Section 7 concludes the paper.

[2] The work in this paper was presented in part in the IEEE International Conference on Communications (ICC) 2019 [36].

1.3 Notation

Vectors are denoted by bold lowercase letters and random vectors by bold uppercase letters, respectively (e.g., $\mathbf{x}$, $\mathbf{X}$). We denote the distribution of a random vector $\mathbf{X}$ by $P_{\mathbf{X}}$. If $\mathbf{X}, \mathbf{Y}$ are two random vectors equal in distribution, then we write $\mathbf{X} \overset{d}{=} \mathbf{Y}$.

Let $\mathbf{X}$ and $\mathbf{Y}$ be continuous random vectors on $\mathbb{R}^d$ with distributions $P_{\mathbf{X}}$ and $P_{\mathbf{Y}}$, respectively. The density of $\mathbf{X}$ is denoted by $p_{\mathbf{X}}$ and the density of $\mathbf{Y}$ by $p_{\mathbf{Y}}$. Then, the KL divergence between $\mathbf{X}$ and $\mathbf{Y}$ is defined by

$$D_{KL}(P_{\mathbf{X}}||P_{\mathbf{Y}}) = \int_{\mathbb{R}^d} p_{\mathbf{X}}(\mathbf{x}) \log \frac{p_{\mathbf{X}}(\mathbf{x})}{p_{\mathbf{Y}}(\mathbf{x})} d\mathbf{x}. \tag{1}$$

Let $f : \mathbb{R} \to \mathbb{R}$ and $g : \mathbb{R} \to \mathbb{R}$. We use the Landau notation where $f(x) = o(g(x))$ if $\lim_{x\to\infty} \frac{f(x)}{g(x)} = 0$.

2 System model

2.1 Spatial location

Consider a network of devices located according to a general point process, denoted by Φ. These devices form interferers for a desired receiver located at the origin associated with a single desired transmitter. We focus on three models for Φ (precise definitions can be found in [37]):

1. *HPPP* with intensity λ devices per m^2;
2. *Doubly Poisson cluster process*: the parent point process is a HPPP with intensity λ_p devices per m^2, and each daughter process, centered on its parent's position, is also a HPPP with intensity λ_d devices per m^2 restricted to a disc of radius r_c. Points from the parent HPPP are included.[3] Hence, the average number of points in each cluster is $c = \lambda_d \pi r_c^2 + 1$ devices.
3. *Matérn hard-core process of type II*: the underlying HPPP is with intensity λ_p devices per m^2, and the hard-core distance is r_h.

These three point processes are representative of a large family of processes. In the first case, the HPPP exhibits uniform behavior in the sense that conditioned on the number of points in a region, each point is uniformly and independently distributed in the region. On the other hand, the doubly Poisson cluster process exhibits attraction, while the Matérn hard-core process of type II exhibits repulsion. We remark that these models can capture device clustering due to human activity as well as the activity of devices under both duty cycle constraints and, in the case of the Matérn hard-core process, CSMA-type protocols [7].

In each case, the intensity—e.g., λ in the case of the HPPP—corresponds to the intensity of active devices with data to transmit. In 5G, a common target is one device per m^2; however, the density of active devices with a given protocol, in a given time frame and

[3] We remark that a standard formulation of the doubly Poisson cluster process studied in [6], known as the Neyman-Scott process, does not include the parent process points. However, doing so enables the development of the rigorous approximation theorems in Sect. 3.

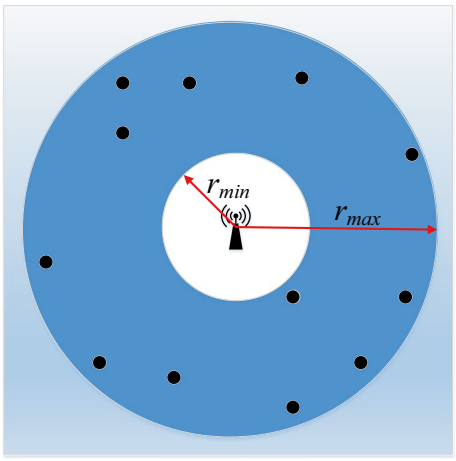

Fig. 1 Illustration of a finite radius network consisting of a receiver with a non-zero guard zone

spectrum band, may be significantly lower. We will often set $\lambda \in [0.001, 0.01]$ devices per m^2.

We assume that the radius of the network, $r_{\max}$, is finite and that there is a guard zone; i.e., a minimum distance between the receiver and the closest interferer, $r_{\min}$ (see Fig. 1). This assumption is introduced due to the fact that interferers cannot be arbitrarily close to the receiver (e.g., due to the fact a receiver has non-zero area), and interferers cannot be arbitrarily far away in realistic models.

$$\Gamma(r_{\min}, r_{\max}) = \{\mathbf{x} \in \mathbb{R}^2 : r_{\min} \leq \|\mathbf{x}\| \leq r_{\max}\}. \tag{2}$$

Restricting Φ to this annulus yields a new point process, which is denoted by

$$\Phi_{\Gamma(r_{\min}, r_{\max})} = \Phi \cap \Gamma(r_{\min}, r_{\max}). \tag{3}$$

2.2 Channel access

Motivated by the NB-IoT protocol, we assume that the desired transmitter and all interferers utilize OFDM with the same symbol period. In particular, the desired transmitter communicates using NK subcarriers to an already associated desired receiver. On the other hand, the interferers randomly access a subset of the NK subcarriers for their transmissions.

We assume that the subcarriers that each interferer can access are grouped into K distinct blocks of N subcarriers, known as a minimum size block (msB). That is, if an interfering device selects a msB, denoted by $B_u = \{b_{u,1}, \ldots, b_{u,N}\}$ where $b_{u,i}$ is the i-th subcarrier of the msB B_u, then all of the N subcarriers in B_u are utilized. The complete set of all subcarriers is denoted by $\mathcal{B} = \cup_{u=1}^{K} B_u$.

The decision of an interferer of which subcarriers are utilized is made individually without coordination with any other device in the network. In particular, the interferer randomly selects each msB independently with probability p. The probability p is dependent on the needs of the transmitting device; i.e., the higher the required rate, the

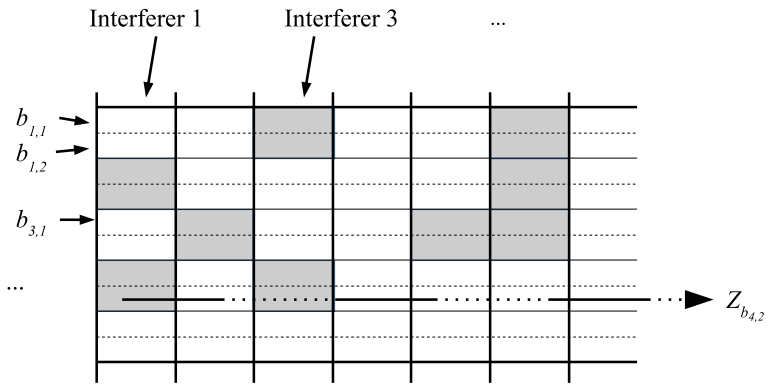

Fig. 2 Illustration of the channel access. The set of 10 subcarriers is considered, with $K = 5$ msBs of size $N = 2$. $b_{u,i}$ is the i-th subcarrier from the u-th msB, $u = 1, \ldots, 5$. The contribution of each interferer in msBs is shown with gray indicating that the device is active. The resulting interference is a complex vector with NK elements. The element $Z_{u,i}$ corresponds to the sum of all contributions falling in the subcarrier $b_{u,i}$

larger the value of p. The effect of p is to introduce sporadic transmissions in the frequency domain, analogous to existing work in the time domain [38]. In this paper, we assume that p is constant for all interfering devices.

The interference at the desired receiver on a given msB B_u is the sum of all interference from each interfering device that accesses B_u. An illustration is provided in Fig. 2 with $K = 5$ msBs with $N = 2$ subcarriers in each msB. We also note that our setup corresponds to a wide range of protocols. For example, in many currently implemented LPWAN protocols, grouping of subcarriers is not yet available. In this case, each msB consists of a single subcarrier; i.e., $N = 1$. On the other hand, in the NB-IoT standard for uplink transmissions (NPUSCH) [10], each msB can contain up to $N = 12$ subcarriers with a 15 kHz spacing, which can also be captured within our model.

2.3 Interference signal

Consider a subcarrier $b_{u,i}$ associated with the msB B_u. Under a power-law path loss model, the interference observed by the receiver at the origin on this subcarrier is given by

$$Z_{b_{u,i}} = \sum_{j \in \Phi_{b_{u,i}}} r_j^{-\frac{\eta}{2}} h_{j,b_{u,i}} x_{j,b_{u,i}}, \tag{4}$$

where r_j is the distance from device j to the origin, $\eta > 2$ is the path-loss exponent, $h_{j,b_{u,i}}$ is the fading coefficient for device j on subcarrier $b_{u,i}$, and $x_{j,b_{u,i}}$ is the baseband emission. Implicit in (4) is the assumption that the desired receiver has a symbol period consistent with the interferers in order to guarantee orthogonality of the subcarrier signals. While we do not pursue relaxing this assumption in this paper, we note that mismatched sampling in the desired link for single-carrier systems with α-stable noise has been investigated in [39].

After stacking the interference on each subcarrier for each msB, the resulting interference random vector is given by

$$\mathbf{Z} = \left[\mathrm{Re}(Z_{b_{1,1}}), \mathrm{Im}(Z_{b_{1,1}}), \ldots, \mathrm{Re}(Z_{b_{K,N}}), \mathrm{Im}(Z_{b_{K,N}})\right]^T. \tag{5}$$

The study of the interference random vector $\mathbf{Z}$ is the focus of this paper. It is known that under the assumptions in this section, each pair $(\mathrm{Re}(Z_{b_{u,i}}), \mathrm{Im}(Z_{b_{u,i}}))$ has a log-characteristic function given in [6, Eq. (13)]. However, this representation is analytically intractable and not amenable to the study of the random vector $\mathbf{Z}$ in (5). As such, we investigate alternative approximations of the marginal distributions in the following section.

3 Multivariate interference statistics

In this section, we develop statistical models for the interference amplitude and phase statistics when multiple subcarriers are utilized. That is, we introduce approximate probability distributions for the random vector in (5). Our models are based on the assumption that device locations are governed by a HPPP, which induce α-stable models that we overview in Appendix A. We also show that similar approximations can also be applied to certain non-Poisson point processes.

3.1 Interference characterization

We now derive a general and tractable approximate characterization for the multivariate interference $\mathbf{Z}$ in (5) induced by HPPPs. The main difficulty in obtaining a tractable characterization of the interference is the complex statistical dependence structure of $\mathbf{Z}$. There are two issues, elaborated on further in the sequel, that must be addressed:

(i) The in-phase and quadrature interference for a single subcarrier (i.e., a single element of $\mathbf{Z}$) induced by a HPPP is heavy-tailed; namely symmetric α-stable with infinite variance. As a consequence, the dependence cannot be adequately described via the correlation, as in Gaussian models.

(ii) Under the assumptions in this paper, the joint distribution of the interference for a single subcarrier induced by a HPPP is isotropic sub-Gaussian α-stable [40]. Moreover, partial overlaps in the subcarriers used by each device induce an even more complicated dependence structure. As such, a full characterization of the joint probability density function for $\mathbf{Z}$ is in general intractable.

To address the issues (i)-(ii), a general technique developed in statistics—albeit only sparingly used in signal processing—is to decouple the characterization of the individual elements (marginal laws) of the random vector $\mathbf{Z}$ from the dependence structure. This general approach can be understood by considering the joint distribution function of a continuous random vector in $\mathbb{R}^n$, say $\mathbf{X} = [X_1, \ldots, X_n]^T$. By Sklar's theorem [31], this approach can be rigorously justified as the joint distribution of $\mathbf{X}$ can always be uniquely written in the form

$$F(x_1, \ldots, x_n) = C(F_1(x_1), \ldots, F_n(x_n)), \tag{6}$$

where $C : [0,1]^n \to [0,1]$ is called a *copula function*, and F_i, $i = 1, \ldots, n$ are the marginal distribution functions. When both the joint and marginal distributions admit density functions (as is the case in the interference models considered in this paper), the joint probability density function has the form

$$p_{\mathbf{X}}(x_1,\ldots,x_n) = \underbrace{c(F_1(x_1),\ldots,F_n(x_n))}_{\text{dependent component}} \underbrace{\prod_{i=1}^{n} p_{X_i}(x_i)}_{\text{independent component}}. \tag{7}$$

That is, the joint probability density function decomposes into the product of the marginal densities and another density function $c : [0,1]^n \to \mathbb{R}_+$, which captures dependence between the different components of $\mathbf{X}$ and is scale-free.

To apply the copula approach, we first require characterization of the individual elements of $\mathbf{Z}$. For interference induced by a HPPP defined on $\mathbb{R}^2$, we exploit the following result obtained in [6, 13–15] (given in this form in [40]).

Theorem 1 *Consider the interference on subcarrier $b_{u,i}$ in msB B_u induced by a HPPP with intensity λ, denoted by $Z_{b_{u,i}}$ in (4). Suppose that $h_{j,b_{u,i}} x_{j,b_{u,i}}$ in (4) is an isotropic complex random variable and*

$$\mathbb{E}[|\mathrm{Re}(h_{j,b_{u,i}} x_{j,b_{u,i}})|^{4/\eta}] < \infty, \tag{8}$$

with $\eta > 2$. Then, $Z_{b_{u,i}}$ in (4) converges almost surely to an isotropic $4/\eta$-stable random variable. Moreover, the scale parameters of real and imaginary components are equal, given by

$$\gamma_{Z_{b_{u,i}}} = \left(\pi \lambda p C_{4/\eta}^{-1} \mathbb{E}[|\mathrm{Re}(h_{j,b_{u,i}} x_{j,b_{u,i}})|^{4/\eta}]\right)^{\eta/4}, \tag{9}$$

where

$$C_\alpha = \begin{cases} \frac{1-\alpha}{\Gamma(2-\alpha)\cos(\pi\alpha/2)}, & \text{if } \alpha \neq 1 \\ 2/\pi, & \text{if } \alpha = 1. \end{cases} \tag{10}$$

Remark 1 The parameters of the interference distribution given in Theorem 1 depend on physical variables, including the device intensity λ, the service rate p, the path-loss exponent η.

By Theorems 3 and 4, the result in Theorem 1 also forms a good approximation of the marginal distributions for interference induced by doubly Poisson cluster processes and Matérn hard-core processes of type II defined on $\mathbb{R}^2$. For a sufficiently small guard zone and sufficiently large network radii, $r_{\min}$ and $r_{\max}$ respectively, it is also known for interference induced by a HPPP restricted to the annulus $\Gamma(r_{\min}, r_{\max})$, Theorem 1 is a good approximation for the marginal interference distribution [6]. We further investigate the impact of the restriction to an annulus in Sect. 5.

The next step is to select an appropriate copula function C. There are two aspects of the copula model to consider: accuracy and tractability. As we will show in Sect. 5, t-copula models form a good approximation of the dependence structure of $\mathbf{Z}$ for a wide range of network parameters. Such t-copula models also admit very low-complexity parameter estimation algorithms, which will be developed in Sect. 4. Finally, t-copula models are simple to simulate exactly via scale mixture decompositions, which provides a useful tool in evaluating performance (as carried out in Sect. 6).

To describe the t-copula model, let F_ν be the distribution of the univariate t-distribution, given by

$$F_\nu(x) = \int_{-\infty}^{x} \frac{\Gamma(\frac{\nu+1}{2})}{\sqrt{\nu\pi}\Gamma(\frac{\nu}{2})}\left(1+\frac{t^2}{\nu}\right)^{-\frac{\nu+1}{2}} \mathrm{d}t, \tag{11}$$

parameterized by the degree of freedom $\nu \in \mathbb{R}^+$. Moreover, the joint distribution $F_{\nu,\Sigma}$ of a n-dimensional multivariate t-distribution is given by

$$F_{\nu,\Sigma}(\mathbf{x}) = \int_{-\infty}^{x_1} \cdots \int_{-\infty}^{x_n} \frac{\Gamma(\frac{\nu+d}{2})}{\Gamma(\frac{\nu}{2})\sqrt{(\pi\nu)^d|\Sigma|}}\left(1+\frac{\mathbf{t}^T\Sigma^{-1}\mathbf{t}}{\nu}\right)^{-\frac{\nu+d}{2}} \mathrm{d}\mathbf{t}, \tag{12}$$

parameterized by the degree of freedom $\nu \in \mathbb{R}_{\geq 0}$ and the $n \times n$ correlation matrix Σ.

The t-copula is then defined as

$$C^t_{\nu,\Sigma}(\mathbf{u}) = F_{\nu,\Sigma}(F_\nu^{-1}(u_1), \ldots, F_\nu^{-1}(u_n))). \tag{13}$$

That is, the t-copula captures the dependence structure of a multivariate t-distribution without necessarily having t-distributed marginals; i.e., a meta-t distribution [41, 42]. In particular, (13) can be used in (6) to construct multivariate distributions with the symmetric α-stable marginals obtained in Theorem 1. This provides a basis to tractably model the interference random vectors arising from the system model in Sect. 2.

We highlight that the t-copula α-stable model resolves the issues (i)–(ii) at the beginning of this subsection. With respect to (i), the heavy-tailed nature of the interference is captured by the use of symmetric α-stable marginals, motivated by Theorem 1. Moreover, the complex dependence structure resulting in issue (ii) is captured through the t-copula parameters ν, Σ, which can be efficiently estimated. As such, there is not a significant increase in the complexity of the model compared with Gaussian models, as instead of covariance there are the parameters of the symmetric α-stable marginals and ν, Σ.

3.2 Multivariate interference characterization with $p = 1$

Before establishing low-complexity parameter estimation algorithms and verifying the approximate t-copula model, we derive the exact multivariate interference distribution induced by a HPPP for a single msB or when $p = 1$ (recall from Sect. 2 that p is the activity probability) in Rayleigh fading. This result will aid verification of the t-copula model in this regime and provide insight into symbol detection rules in Sect. 6.

To this end, let $\mathbf{Z}_{B_u}$ denote the interference on all subcarriers for a given msB B_u induced by a HPPP on $\mathbb{R}^2$; that is,

$$\mathbf{Z}_{B_u} = [\mathrm{Re}(Z_{b_{u,1}}), \mathrm{Im}(Z_{b_{u,1}}), \ldots, \mathrm{Re}(Z_{b_{u,N}}), \mathrm{Im}(Z_{b_{u,N}})]^T. \tag{14}$$

The following theorem provides a characterization of the interference random vector $\mathbf{Z}_{B_u}$. Recall that if a device transmits on a subcarrier within a msB B_u, then it transmits on all subcarriers in B_u so that the set of interferers remains unchanged on all subcarriers. In this special case, the interference random vector in (14) can be characterized exactly as shown in the following theorem.

Theorem 2 *Let $j \in \Phi_{B_u}$ be a point of a HPPP on $\mathbb{R}^2$ with intensity λ. Suppose that $h_{j,b_{u,i}} \sim \mathcal{CN}(0,1)$ (Rayleigh fading), $\mathrm{Re}(x_{j,b_{u,i}}) \sim \mathrm{Unif}(\{+1,-1\})$, $\mathrm{Im}(x_{j,b_{u,i}}) \sim \mathrm{Unif}(\{+1,-1\})$, and that the conditions in Theorem 1 hold. Then, the interference random vector $\mathbf{Z}_{B_u}$ follows the sub-Gaussian α-stable distribution with an underlying Gaussian vector having i.i.d. $\mathcal{N}(0,\sigma^2_{\mathbf{Z}_{B_u}})$ components, $\alpha = 4/\eta$ and parameter*

$$\gamma_{\mathbf{Z}_{B_u}} = \left(\pi \lambda p C^{-1}_{4/\eta} \mathbb{E}[|\mathrm{Re}(h_{j,b_{u,1}} x_{j,b_{u,1}})|^{4/\eta}]\right)^{\eta/4}, \tag{15}$$

where $\gamma_{\mathbf{Z}_{B_u}} = \frac{1}{\sqrt{2}}\sigma_{\mathbf{Z}_{B_u}}$ and $C_{4/\eta}$ is given in (10). Furthermore, suppose $p = 1$. Then, the interference random vector $\mathbf{Z}$ in (5) is also sub-Gaussian α-stable with an underlying Gaussian vector having i.i.d. $\mathcal{N}(0,\sigma^2_{\mathbf{Z}_B})$ components, $\alpha = 4/\eta$.

Proof See Appendix B. □

Remark 2 As for Theorem 1, the parameters of the interference distribution given in Theorem 2 depend on physical variables, including the device intensity λ, the service rate p, the path-loss exponent η.

We point out that the sub-Gaussian α-stable random vectors arising in Theorem 2 are isotropic, and lie in the family of elliptical distributions [43]. As t-copula models also yield elliptical distributions, it follows that the t-copula model should be a good approximation of the multivariate interference distribution when $p \approx 1$. We validate this observation in Sect. 5.

3.3 Non-Poisson models

So far in this section, we have assumed that device locations are governed by a HPPP. A natural question is whether similar models are also accurate for non-Poisson point processes. To this end, consider the families of doubly Poisson cluster processes (as defined in Sect. 2) and Matérn hard-core type II processes. As these processes are constructed from HPPP, it would suggest that for sufficiently small values of the intensity of the daughter process for doubly Poisson cluster processes or the hard-core distance for the Matérn hard-core type II processes, the induced interference may be approximated by the interference induced by a HPPP.

We establish that such an approximation indeed holds in the sense of convergence in distribution. In other words, the distribution of the interference induced by these more general families of point processes and the distribution of the interference induced by a HPPP have a small Lévy–Prokhorov metric [44]. This result is given in the following theorems.

Theorem 3 *Let* $\Phi^{\lambda_d,\lambda_p,r_c}_{\Gamma(r_{\min},r_{\max})}$ *be a doubly Poisson cluster process with parameters* $\lambda_d, \lambda_p, r_c$. *Suppose that for all subcarriers* $b_{u,i}$ *the random variables* $h_{j,b_{u,i}}x_{j,b_{u,i}}$ *defined in* (4) satisfy the condition that $\mathrm{supp}(h_{j,b_{u,i}}x_{j,b_{u,i}})$ *is compact. Then, the induced interference random vector in* (5) *converges in distribution to the interference random vector induced by a HPPP restricted to* $\Gamma(r_{\min}, r_{\max})$ *as* $\lambda_d \to 0$.

Proof See Appendix C. □

Theorem 4 *Let* $\Phi^{r_h,\lambda_p}_{\Gamma(r_{\min},r_{\max})}$ *be a Matérn hard-core process of type II with parameters* r_h, λ_p. *Suppose that for all subcarriers* $b_{u,i}$ *the random variables* $h_{j,b_{u,i}}x_{j,b_{u,i}}$ *defined in* (4) satisfy the condition that $\mathrm{supp}(h_{j,b_{u,i}}x_{j,b_{u,i}})$ *is compact. Then, the induced interference random vector in* (5) *converges in distribution to the interference random vector induced by a HPPP restricted to* $\Gamma(r_{\min}, r_{\max})$ *as* $r_h \to 0$.

Proof See Appendix C. □

Theorems 3 and 4 implies that for sufficiently small λ_d, r_h as well as a wide range of fading and baseband emission models, both the doubly Poisson cluster process and the Matérn hard-core type II process induce interference that can be well approximated by that of a HPPP in the sense that the resulting interference distribution is close in the sense of the topology of weak convergence or, equivalently, the Lévy-Prokhorov metric.

This suggests that models developed for interference arising from a HPPP will also be useful for doubly Poisson cluster and Matérn hard-core type II processes when λ_d, r_h are sufficiently small. Further discussion on the quality of this approximation will be presented via the numerical study in Sect. 5.

4 Parameter estimation for multivariate interference

The utility of the model proposed in Sect. 3 depends heavily on whether low-complexity parameter estimation algorithms are available. In general, particularly in high dimensions, maximum likelihood estimation for t-copula models is computationally demanding [45].

In this section, we propose a new low-complexity algorithm to estimate parameters for the t-copula interference model. Our algorithm tailors a general estimation method for copula models, known as inference from the margins [46], to the specific model derived in Sect. 3. In the remainder of this section, we first overview the inference from the margins method for general t-copula models. We then detail our proposed low-complexity parameter estimation method exploiting the structure of the interference model.

4.1 Copula parameter estimation

A standard approach for parameter estimation in t-copula models, known as inference from the margins, proceeds as follows [46, 47]. Consider a d-dimensional random vector $\mathbf{X} = [X_1, \ldots, X_d]^T$ on $\mathbb{R}^d$ governed by a t-copula with parameters ν, Σ.

According to [48], the elements of Σ can be obtained via Kendall's τ rank correlation, denoted as ρ_τ. Let $\mathbf{X}_i = [X_{i,1}, \ldots, X_{i,d}]^T$, $i = 1, \ldots, n$ be n independent samples of $\mathbf{X}$. A natural estimator for Σ is then given by [45]:

$$\hat{\Sigma}_{jk} = \sin\left(\frac{\pi}{2}\hat{\rho}_\tau(X_j, X_k)\right), \tag{16}$$

where

$$\hat{\rho}_\tau(X_j, X_k) = \binom{n}{2} \sum_{1 \le i_1 \le i_2 \le n} \operatorname{sign}\big((X_{i_1,j} - X_{i_2,j})(X_{i_1,k} - X_{i_2,k})\big). \tag{17}$$

In general, there are no guarantees that $\hat{\Sigma}$ is positive definite, nevertheless, it is possible to apply adjustment techniques [49] to ensure positive definiteness. Having estimated Σ, the standard approach then obtains the degree of freedom ν via maximum likelihood estimation given Σ [45].

An alternative method for estimating the degree of freedom also exists based on the tail dependence. In particular, consider a bivariate random vector (X_1, X_2) with marginal distributions F_1, F_2, respectively. Then, the (upper) tail dependence $\lambda_{\mathbf{X}}$ is defined by

$$\lambda_{\mathbf{X}} = \lim_{u \to 1} \Pr\Big(X_1 > F_1^{-1}(u) | X_2 > F_2^{-1}(u)\Big). \tag{18}$$

In the case that (X_1, X_2) is governed by a t-copula, [45, Proposition 1] provides a link between the tail dependence and the degree of freedom ν. For a random vector $\mathbf{X}$, if the tail dependence is known to be constant amongst each pair of elements in $\mathbf{X}$ and the off-diagonal elements of Σ are a constant value ρ, then the degree of freedom ν can be obtained from the tail dependence $\lambda_{\mathbf{X}}$ via [45]

$$\lambda_{\mathbf{X}} = 2F_{\nu+1}\left(\frac{\sqrt{1+\nu}\sqrt{1-\rho}}{\sqrt{1+\rho}}\right). \tag{19}$$

where $F_{\nu+1}$ is defined in (11) with degree of freedom $\nu + 1$.

4.2 A low-complexity estimation procedure

We now develop a new parameter estimation algorithm for the t-copula interference model. Our approach is based on inference from the margins, where we require estimates of the tail dependence $\lambda_{\mathbf{Z}}$ to obtain the degree of freedom ν, and the correlation matrix Σ. In particular, we derive the following approximation—detailed in Appendix D—for the tail dependence, $\lambda_{\tilde{\mathbf{Z}}}$, and the correlation matrix Σ:

$$\lambda_{\tilde{\mathbf{Z}}} \approx \frac{2p}{\mathbb{E}\left[|(Z_{1,1})|^{\frac{4}{\eta}}\right]} \int_0^\infty (1 - F_{Z_{1,1}}(z))^2 \frac{4}{\eta} z^{\frac{4}{\eta}-1} \mathrm{d}z, \qquad \Sigma \approx \mathbf{I}_{2KN}. \tag{20}$$

where $Z_{1,1} = \mathrm{Re}(h_{1,1}x_{1,1})$.

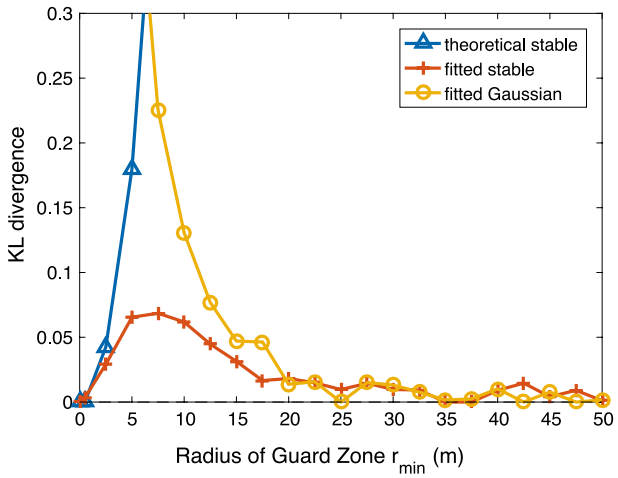

Fig. 3 Plot of the KL divergence between the simulated data set from HPPP and three statistical models (under different guard-zone radii): theoretical stable model ($\alpha = 4/\eta$); fitted stable model ($\hat{\alpha}$); and fitted Gaussian model

Algorithm 1 Proposed Copula Parameter Estimation Algorithm

Input: S independent samples of the interference random vector $\mathbf{Z}^1, \ldots, \mathbf{Z}^S$
Output: Correlation matrix Σ and degree of freedom ν
Process:
1: Estimate the parameters of the α-stable marginals, α, γ (see, e.g., [50])
2: Set the correlation matrix for the t-copula model $\Sigma = \mathbf{I}_{2KN}$
3: Set the tail dependence for the t-copula model to be $\lambda_{\mathbf{Z}}$ in (20)
4: Compute the degree of freedom ν for the t-copula model via (19)

Our interference parameter estimation algorithm is given in Algorithm 1. The first step is to estimate the exponent and scale parameter of the symmetric α-stable marginals motivated by Theorem 1, which can be achieved using standard methods (see, e.g., [50] under the assumption of independent observations of the interference random vector $\mathbf{Z}$. Assuming that the lifetime of device transmissions is not long (as is typical in NB-IoT networks), these samples can be collected from nearly consecutive frames.

Lines 2-4 in Algorithm 1 are concerned with estimation of the t-copula parameters ν and Σ. Indeed, these steps only require the computation in (20) when the fading statistics and path-loss exponent are known. This contrasts with the estimation of general t-copula models (i.e., without the structure of the interference random vector $\mathbf{Z}$), where a large number of samples are required. A detailed numerical study of the quality of the approximation is carried out in the following section.

5 Results and discussion: model verification

In this section, we compare the interference models developed in Sect. 3 with the interference arising from the scenarios detailed in Sect. 2 based on the KL divergence, which can be viewed as a distance between two probability distributions. The KL divergence therefore provides additional insights into the statistics of the interference, particularly when multiple subcarriers experience large amplitude interference. In each scenario, we

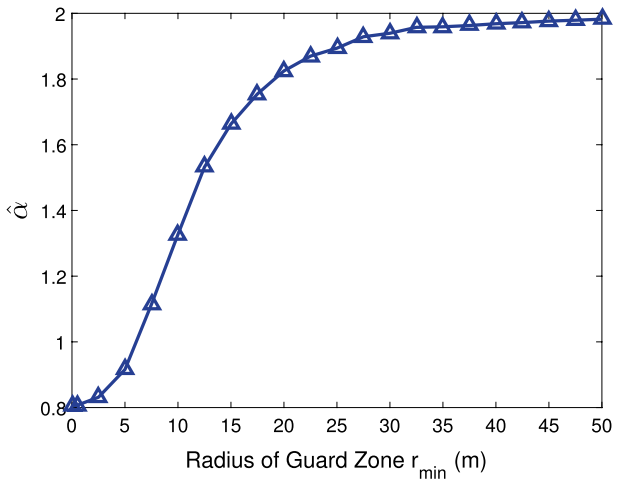

Fig. 4 Fitted stable parameter—$\hat{\alpha}$ under different guard-zone radii in HPPP

assume that that the baseband emission of each interferer is uniformly distributed on $\{-1, +1\}$ with Rayleigh fading, as in Theorem 2.

5.1 Interference on a single subcarrier

We first verify that an α-stable model is accurate for HPPPs with non-zero guard zones. Consider the HPPP $\Phi_{\Gamma(r_{\min},500)}$ with path-loss exponent $\eta = 5$ and intensity $\lambda = 0.001$ devices per m^2. Figure 3 plots the impact of varying $r_{\min}$ on the KL divergence between the simulated interference and three different models for a single subcarrier: the α-stable model that assumes no guard zone (theoretical stable); an α-stable model with parameters estimated from a set of simulated data; and a fitted Gaussian model.

Observe that for a very small $r_{\min}$, the theoretical model exhibits a good fit while for $r_{min} > 15$ m, the Gaussian model is a good fit. Moreover, the symmetric α-stable model with an estimated exponent $\hat{\alpha}$ obtained using the method in [50], yields a low KL divergence, while the others do not. As shown in Fig. 4, the parameter $\hat{\alpha}$ increases from approximately $4/\eta = 0.8$ to nearly 2 as $r_{\min}$ ranges from 0.5 m to 50 m. As such, α-stable models with estimated exponent $\hat{\alpha}$ are robust to changes in $r_{\min}$—implying that the techniques in this paper hold rather generally—with the qualification that the best choice of α may be larger than $4/\eta$ as predicted by Theorem 1.

5.2 Interference random vector model

We now turn to our model for the interference random vector developed in Sect. 3.2. We numerically investigate[4] the behavior of our proposed models by evaluating the KL divergence between the interference arising from the scenario in Sect. 2 and our models in Sect. 3. That is, we estimate $D_{KL}(P||Q)$ where P is the distribution corresponding to the system model in Sect. 2 and Q is the distribution arising from our models. The interference random vector has in general a high dimension ($2KN$ dimensions for K msBs and

[4] Estimation of the α-stable marginal parameters is carried out using [51].

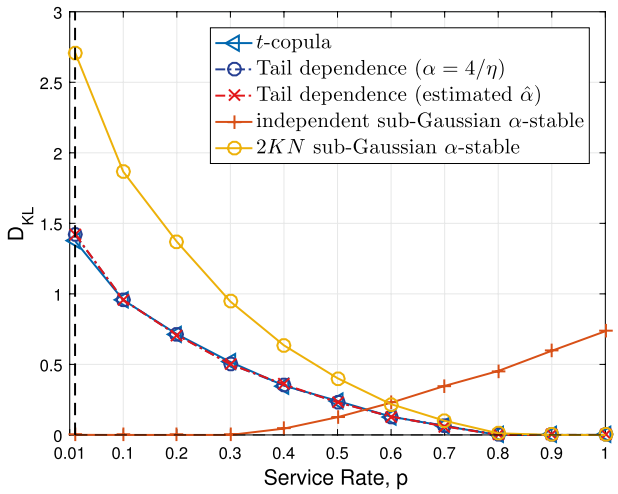

Fig. 5 Plot of the KL divergence between the simulated data set and five statistical models (under HPPP): *t*-copula model (maximum likelihood); Algorithm 1 based on $\alpha = 4/\eta$; Algorithm 1 based on estimated $\hat{\alpha}$; independent sub-Gaussian α-stable model; and $4K$ sub-Gaussian α-stable model. In the figure, $K = 4$ msBs and $N = 2$ subcarriers in each msB are considered

N subcarriers in each msB as detailed in Sect. 2). As such, even the numerical evaluation is non-trivial, and we use the k-nearest neighbor method implemented in the MATLAB package [52] for the computation of the KL divergence.

All figures are generated using a simulated data set with 80, 000 samples. Due to the high dimension of the interference random vector, the k-nearest neighbor method can output very small negative values [53]. In the figures, these negative values are rounded to zero.

In the following numerical results, we compare five models all with α-stable marginal distributions motivated by Theorem 2 in Figs. 5, 6 and 7:

1 The *t*-copula α-stable model detailed in Sect. 3.2 with three different parameter estimation algorithms: *a)* via maximum likelihood estimation; *b)* via Algorithm 1 with $\alpha = 4/\eta$; *c)* via the low-complexity estimation procedure for *t*-copula parameters as Algorithm 1 while using the estimated $\hat{\alpha}$ in (20).
2 The independent sub-Gaussian α-stable model consisting of independent $2N$-dimensional sub-Gaussian α-stable random vectors. In this model, the $2KN$-dimensional random interference vector $\mathbf{Z}$ is decomposed into K $2N$-dimensional random vectors (corresponding to the real and imaginary parts of the N subcarriers on each msB). Each $2N$-dimensional random vector is sub-Gaussian α-stable (see Definition 2) and independent of each of the other $K-1$ N-dimensional random vectors. This model is exact when interfering devices only transmit on a single subcarrier, the guard-zone radius $r_{\min} = 0$, and the network radius $r_{\max} \to \infty$.

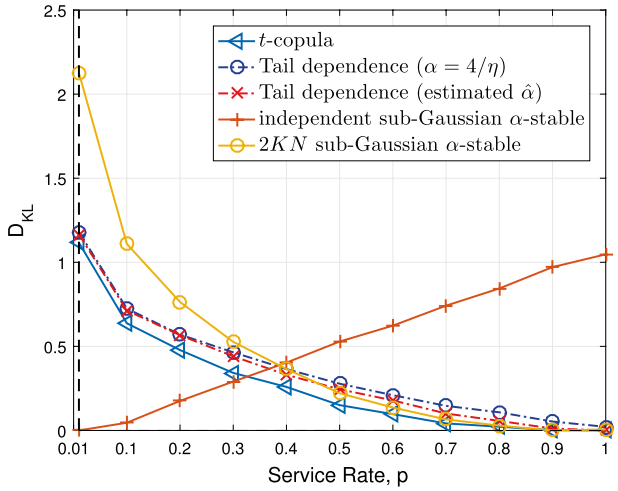

Fig. 6 Plot of the KL divergence between the simulated data set and five statistical models (under doubly Poisson cluster process): *t*-copula model (maximum likelihood); Algorithm 1 based on $\alpha = 4/\eta$; Algorithm 1 based on estimated $\hat{\alpha}$; independent sub-Gaussian α-stable model; and $4K$ sub-Gaussian α-stable model. In the figure, $K = 4$ msBs and $N = 2$ subcarriers in each msB are considered

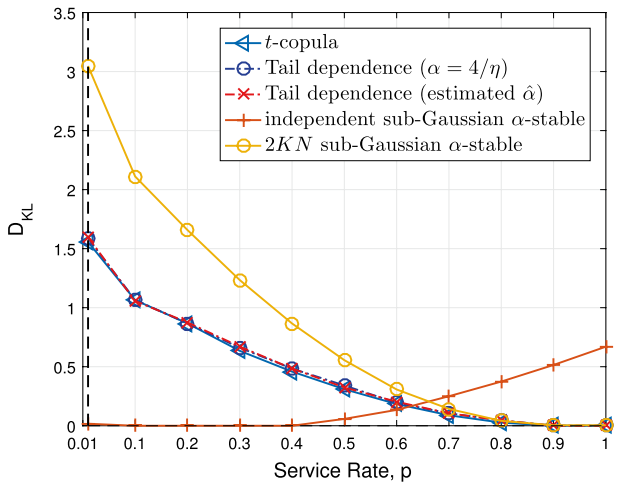

Fig. 7 Plot of the KL divergence between the simulated data set and five statistical models (under Matérn hard-core process of type II): *t*-copula model (maximum likelihood); Algorithm 1 based on $\alpha = 4/\eta$; Algorithm 1 based on estimated $\hat{\alpha}$; independent sub-Gaussian α-stable model; and $4K$ sub-Gaussian α-stable model. In the figure, $K = 4$ msBs and $N = 2$ subcarriers in each msB are considered

3 The $2KN$ sub-Gaussian α-stable model consisting of a $2KN$-dimensional sub-Gaussian α-stable random vector. This model corresponds to the scenario where all devices transmit on every msB in $\mathcal{B}$; i.e., $p = 1$ (see Theorem 2).

In the following, we set $K = 4$ msBs and $N = 2$ subcarriers in each msB, $r_{\min} = 0$, $r_{\max} = \infty$, $\eta = 3$, $h_{j,b_i} \sim \mathcal{CN}(0,1)$, and $x_{j,b_{u,i}}$ is uniformly drawn from $\{-1,1\}$, $\forall j, b_{u,i}$.

Table 1 Parameters for doubly Poisson point process and Matérn hard-core process point process

Doubly Poisson			**Matérn Hard-core**	
λ_p (devices per m^2)	r_c (m)	λ_d (devices per m^2)	λ (devices per m^2)	r_h (m)
2×10^{-4}	30	$10/(\pi r_c^2) = 0.0035$	2×10^{-4}	20

5.2.1 HPPP

Figure 5 plots the KL divergence between the simulated data set based on the setup in Sect. 2 and the five proposed interference models. We also set $\lambda = 0.001$ devices per m^2. Observe that the $2KN$ sub-Gaussian α-stable model is in good agreement with the simulated data set as $p \to 1$. This is consistent with the characterization in Theorem 2 as when $p \to 1$ all devices transmit on all subcarriers with high probability. On the other hand as p decreases, the $2KN$ sub-Gaussian α-stable model is a poor fit since it cannot capture dependence between interference on different blocks of subcarriers.

Figure 5 also shows that the t-copula model is a good fit for a much larger range of p than the $2KN$ sub-Gaussian α-stable model. As such, it is a good choice for moderately to heavily loaded IoT networks. However, for small p the t-copula model is not satisfactory.

In the lightly loaded scenario where $p \to 0$, each device transmits on more than one msB with a very low probability. By the independent thinning theorem for HPPP, it then follows that the interference on each msB is approximately independent. As a consequence, the independent sub-Gaussian α-stable model is a good choice in the lightly loaded scenario. This observation is verified in Fig. 5, where the KL divergence for this model is nearly zero for small values of p.

5.2.2 Doubly Poisson cluster process

Figure 6 plots the KL divergence for each of the proposed models for locations governed by a doubly Poisson cluster process. The parameters are given in Table 1.

Observe that the t-copula model has a very similar behavior qualitatively consistent with the HPPP case in Fig. 5. This is again consistent with Theorem 3 and also shows that $\lambda_d = 10/(\pi r_c^2)$ is sufficiently small. However, the low-complexity estimation algorithm in Algorithm 1 has reduced performance. This is due to the implicit assumption in the estimation procedure that the void probability is that of a HPPP (see Appendix D for details of the approximation).

5.2.3 Matérn hard-core process of type II

Figure 7 plots the KL divergence for each of the proposed models for locations governed by a Matérn hard-core process of type II. The parameters are given in Table 1.

Observe that the five models have the same performance in terms of KL divergence as under the HPPP. This is consistent with Theorem 3. Moreover, $r_h = 20$ m in Fig. 7 is clearly sufficiently small.

We also note that unlike the doubly Poisson cluster process, the distribution of the closest interferer can also be approximated by (45) [54, Lemma 1]. This provides an explanation for why the low-complexity estimation procedure in Algorithm 1 yields an estimate that well approximates the maximum likelihood estimate.

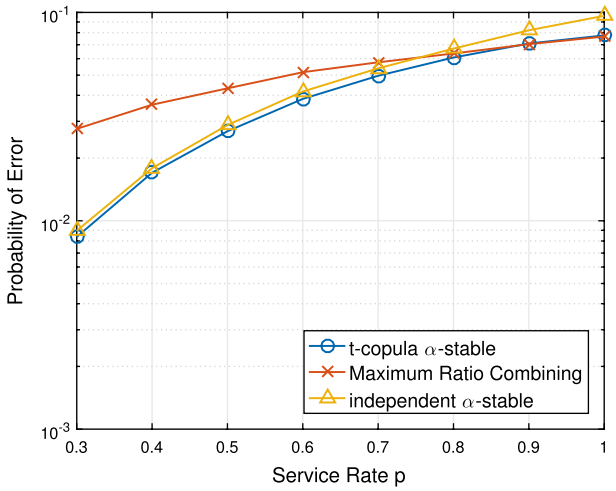

Fig. 8 Probability of error under different service rates, $\eta = 3$, $A = 0.01$ and $\lambda = 0.001$ devices per m^2

6 Receiver design

In this section, we study the impact of the dependence structure on receiver performance using our tractable interference models. We assume that a transmitter seeks to send a binary symbol $x \in \{+1, -1\}$ in the presence of interference arising from one of the scenarios detailed in Sect. 2, with $N = 2$. Given a symbol x, the receiver observes an output $\mathbf{y} \in \mathbb{R}^{2NK}$ defined by

$$\mathbf{y} = \mathbf{g}Ax + \mathbf{z}, \tag{21}$$

where $A = \sqrt{P}r^{-\eta/2}$ is the combination of path loss and transmitted signal, P is the transmitted signal power, $\mathbf{g} \in \mathbb{R}^{2NK}$ corresponds to channel fading after stacking the real and imaginary components of the NK subcarriers and $\mathbf{z} \in \mathbb{R}^{2NK}$ is the interference obtained again by stacking the real and imaginary components of the NK subcarriers, as detailed in Sect. 2. Each subcarrier experiences i.i.d Rayleigh fading; i.e., $\mathbf{g} = [g_1, \cdots, g_{2NK}]$, where $g_i \sim \mathcal{N}(0, 1)$ is i.i.d. We also assume that $\mathbf{g}$ for the desired link is known to the receiver, which is the common scenario where channel estimation is performed.

Given the observation $\mathbf{y}$ and equally likely symbols x, the probability of error is minimized by the likelihood ratio test

$$\Lambda(\mathbf{y}) = \frac{f(\mathbf{y}|x = 1, \mathbf{g})}{f(\mathbf{y}|x = -1, \mathbf{g})} \underset{x=-1}{\overset{x=1}{\gtrless}} 1, \tag{22}$$

where $f(\cdot|x, \mathbf{g})$ is the probability density function of the received signal given that the symbol x is transmitted and the fading is $\mathbf{g}$. As such, different receivers are obtained under the different models introduced in Sect. 3. We therefore consider the following receivers:

1 Based on the t-copula α-stable model detailed in Sect. 3.2.
2 Maximum Ratio Combining (MRC) receiver, which is optimal for Gaussian and sub-Gaussian α-stable models [55].

3 Based on the independent α-stable model [20, 21], where all components of $\mathbf{Z}$ in (5) are assumed to be independent.

To evaluate the different models in terms of the probability of error, we study the impact of the service rate (or access probability) p. Recall that the service rate is the key parameter which controls the dependence between interference on different subcarriers. In our study, we considered the following parameters: $\eta = 3$; $h_{j,b_{u,i}} \sim \mathcal{CN}(0,1)$; $\lambda = 0.001$ devices/m^2; $x_{j,b_{u,i}}$ is uniformly drawn from $\{-1,1\}\ \forall i,j$; $K = 4$; and $N = 2$;

In Fig. 8, the probability of error under each of the different receivers is shown with $A = 0.01$, that is, $P = 10(-4 + \eta \log r)$ (dB) , e.g., $r = 30$ m, $P = 4.3$ dB, based on 200, 000 Monte Carlo iterations. We first observe that when $p \to 1$, the MRC receiver outperforms other receivers due to the fact that it is optimal [55]. However, there is a negligible performance improvement over the t-copula α-stable receiver.

As p decreases, the MRC receiver has poor performance. On the other hand, the t-copula α-stable receiver outperforms receivers tailored to independent α-stable noise [20, 21]. This suggests that the t-copula α-stable receiver is a tractable means of obtaining improved performance for a wide range of network parameters.

7 Conclusions

Motivated by the challenge of multivariate interference in large-scale IoT networks exploiting NB-IoT, we have developed statistical models based on device locations modeled by HPPPs, and copula theory. By evaluating the models in terms of the KL divergence and the probability of error when a desired link exploits a non-linear receiver, we have obtained significant improvements compared to standard approaches which assume independent observations on each subcarrier. Due to the tractability of the models, it is also feasible to rapidly simulate and estimate parameters in order to improve system design.

Appendix A: α-stable model preliminaries

Univariate α-stable models

The α-stable random variables have heavy-tailed probability density functions, which have been widely used to model impulsive signals [56, 57]. The probability density function of an α-stable random variable is described by four parameters: the characteristic exponent $0 < \alpha \leq 2$; the scale parameter $\gamma \in \mathbb{R}_+$; the skew parameter $\beta \in [-1,1]$; and the shift parameter $\delta \in \mathbb{R}$. As such, a common notation for an α-stable random variable X is $X \sim S_\alpha(\gamma,\beta,\delta)$. In the case $\beta = \delta = 0$, X is said to be a symmetric α-stable (SαS) random variable.

In general, α-stable random variables do not have closed-form probability density functions. Instead, they are usually represented by their characteristic function, given by [57, Eq. 1.1.6]

$$\mathbb{E}\left[e^{i\theta X}\right] = \begin{cases} \exp\left\{-\gamma^{\alpha}|\theta|^{\alpha}(1 - i\beta(\text{sign}\theta)\tan\frac{\pi\alpha}{2}) + i\delta\theta\right\}, \alpha \neq 1 \\ \exp\left\{-\gamma|\theta|(1 + i\beta\frac{2}{\pi}(\text{sign}\theta)\log|\theta|) + i\delta\theta\right\}, \alpha = 1 \end{cases} \tag{23}$$

Let $X \sim S_{\alpha}(\gamma, \beta, \delta)$ be an α-stable random variable. A fundamental property of X is the behavior of its probability density function $p_X(x)$ as $x \to \infty$ [57, Theorem 1.2.15]

Theorem 5 *Let $X \sim S_{\alpha}(\sigma, \beta, \delta)$ with $0 < \alpha < 2$, then*

$$\lim_{x\to\infty} x^{\alpha}\Pr(X > x) = C_{\alpha}\frac{1+\beta}{2}\gamma^{\alpha}, \tag{24}$$

where C_{α} is defined in (10).

In the case that X is symmetric α-stable, then $\beta = \delta = 0$ and

$$\Pr(X > x) = \frac{C_{\alpha}}{2}\gamma^{\alpha}x^{-\alpha} + o(x^{-\alpha}). \tag{25}$$

An alternative characterization of symmetric α-stable random variables is the LePage series [57, Theorem 1.4.2]. In particular, let (Γ_i) denote the arrival times of a Poisson process with intensity 1. Let (W_i) be a sequence of symmetric, independent and identically distributed random variables satisfying

$$\gamma = \left(C_{\alpha}^{-1}\mathbb{E}[|W_i|^{\alpha}]\right)^{\frac{1}{\alpha}}, i = 1, 2, \ldots \tag{26}$$

Then,

$$X \overset{d}{=} \sum_{i=1}^{\infty} \Gamma_i^{-\frac{1}{\alpha}} W_i. \tag{27}$$

A key property of the series in (27) following from [57, Page 26], is given as follows.

Property 1 *Let $X \sim S_{\alpha}(\gamma, \beta, \delta)$ and $\Gamma_1^{-\frac{1}{\alpha}} W_1$ be the first term of the Lepage series in (27). Then,*

$$\lim_{x\to\infty} x^{\alpha}\Pr(X > x) = \lim_{x\to\infty} x^{\alpha}\Pr(\Gamma_1^{-\frac{1}{\alpha}} W_1 > x). \tag{28}$$

Sub-Gaussian α-stable random vectors

The notion of an α-stable random vector is defined as follows.

Definition 1 A random vector $\mathbf{X}$ in $\mathbb{R}^d$ is symmetric α-stable if for every $A, B > 0$, there exists a $C > 0$ such that

$$A\mathbf{X}^{(1)} + B\mathbf{X}^{(2)} \overset{d}{=} C\mathbf{X}, \tag{29}$$

where $\mathbf{X}^{(1)}, \mathbf{X}^{(2)}$ are independent copies of $\mathbf{X}$.

We note that each element in $\mathbf{X}$ is an α-stable random variable if $\mathbf{X}$ is an α-stable vector, but not all random vectors with symmetric α-stable marginals form symmetric α -stable random vectors.

A particular class of α-stable random vectors is an instance of the sub-Gaussian α-stable random vectors[5], defined as follows.

Definition 2 Any vector $\mathbf{X}$ distributed as $\mathbf{X} = (A^{1/2}G_1, \ldots, A^{1/2}G_d)$, where

$$A \sim S_{\alpha/2}((\cos \pi\alpha/4)^{2/\alpha}, 1, 0), \tag{30}$$

and $\mathbf{G} = [G_1, \ldots, G_d]^T \sim \mathcal{N}(\mathbf{0}, \sigma^2\mathbf{I})$ is called an isotropic sub-Gaussian α-stable random vector in $\mathbb{R}^d$ with underlying Gaussian vector $\mathbf{G}$. Note that the marginals are symmetric α-stable with scale parameter $\gamma = \frac{1}{\sqrt{2}}\sigma$.

Sub-Gaussian α-stable random vectors also play an important role in studying *complex* α-stable random variables; that is, a random variable with α-stable distributed real and imaginary components. In particular, the generalization of symmetric α-stable random variables to the complex case is known as the class of isotropic α-stable random variables, defined as follows.

Definition 3 Let Z_1, Z_2 be two symmetric α-stable random variables. The complex α -stable random variable $Z = Z_1 + iZ_2$ is *isotropic* if it satisfies the condition

$$e^{i\phi}Z \overset{(d)}{=} Z \text{ for any } \phi \in [0, 2\pi). \tag{31}$$

The following proposition [57, Corollary 2.6.4] highlights the link between isotropic α -stable random variables and sub-Gaussian α-stable random vectors.

Proposition 1 *Let $0 < \alpha < 2$. A complex α-stable random variable $Z = Z_1 + iZ_2$ is isotropic if and only if there are two independent and identically distributed zero-mean Gaussian random variables G_1, G_2 with variance σ^2 and a random variable $A \sim S_{\alpha/2}((\cos(\pi\alpha/4))^{2/\alpha}, 1, 0)$ independent of $(G_1, G_2)^T$ such that $(Z_1, Z_2)^T = A^{1/2}(G_1, G_2)^T$. That is, $(Z_1, Z_2)^T$ is a sub-Gaussian α-stable random vector.*

[5] There exist also sub-Gaussian α-stable random variables that allow for more general dependence structure [57], but they are not necessary for the purposes of this paper.

Appendix B: Proof of Theorem 2

By Theorem 1, the elements of $\mathbf{Z}_{B_u}$ are $4/\eta$-stable random variables with parameter $\sigma_{\mathbf{Z}_{B_u}}$. Consider the first and second components of $\mathbf{Z}_{B_u}$, corresponding to the real and imaginary parts of the interference on the first subcarrier associated to msB B_u. These elements can be written as

$$\begin{aligned} z_{b_{u,1},1} &= \sum_{j\in\Phi_{B_u}} r_j^{-\frac{\eta}{2}} \big(\mathrm{Re}(h_{j,b_{u,1}})\mathrm{Re}(x_{j,b_{u,1}}) - \mathrm{Im}(h_{j,b_{u,1}})\mathrm{Im}(x_{j,b_{u,1}})\big) \\ z_{b_{u,1},2} &= \sum_{j\in\Phi_{B_u}} r_j^{-\frac{\eta}{2}} \big(\mathrm{Re}(h_{j,b_{u,1}})\mathrm{Im}(x_{j,b_{u,1}}) + \mathrm{Im}(h_{j,b_{u,1}})\mathrm{Re}(x_{j,b_{u,1}})\big). \end{aligned} \tag{32}$$

Assume that $h_{j,b_{u,1}} \sim \mathcal{CN}(0,1)$, $\mathrm{Re}(x_{j,b_{u,1}}) \sim \mathrm{Unif}(\{+1,-1\})$, and $\mathrm{Im}(x_{j,b_{u,1}}) \sim \mathrm{Unif}(\{+1,-1\})$. Consider the random vector $\mathbf{Z}^l_{B_u}$, corresponding to the contribution of device $l \in \Phi_{B_u}$ on each subcarrier associated to msB B_u. This can be written as

$$\mathbf{Z}^l_{B_u} = r_l^{-\eta/2}\big(\mathbf{f} \odot \mathrm{Re}(\mathbf{x}_l) + \mathbf{g} \odot \mathrm{Im}(\mathbf{x}_l)\big), \tag{33}$$

where $\odot$ is the Hadamard (element-wise) product. Since $h_{i,b_{u,j}} \sim \mathcal{CN}(0,1)$, it follows that $\mathbf{f} \odot \mathrm{Re}(\mathbf{x}_l)$ and $\mathbf{g} \odot \mathrm{Im}(\mathbf{x}_l)$ are Gaussian random vectors with independent components with the same variance. It then follows that for any orthogonal matrix $\mathbf{U}$ in the set of real orthogonal matrices $\mathcal{O}(2N)$ of dimension $2N \times 2N$,

$$\begin{aligned} \mathbf{U}(\mathbf{f} \odot \mathrm{Re}(\mathbf{x}_l)) &\overset{d}{=} \mathbf{f} \odot \mathrm{Re}(\mathbf{x}_l), \\ \mathbf{U}(\mathbf{g} \odot \mathrm{Im}(\mathbf{x}_l)) &\overset{d}{=} \mathbf{g} \odot \mathrm{Im}(\mathbf{x}_l). \end{aligned} \tag{34}$$

This in turn implies that $\mathbf{U}\mathbf{Z}^l_{B_u} \overset{d}{=} \mathbf{Z}^l_{B_u}$ and hence $\mathbf{U}\mathbf{Z}_{B_u} \overset{d}{=} \mathbf{Z}_{B_u}$, where $\mathbf{U} \in \mathcal{O}(2N)$.

To complete the proof, we apply the following lemma which is a straightforward generalization of [57, Theorem 2.6.3].

Lemma 1 *Let $\mathcal{O}(d)$ be the set of $d \times d$ real orthogonal matrices and $\mathbf{U} \in \mathcal{O}(d)$. Let $\mathbf{Z}$ be an α-stable random vector on $\mathbb{R}^d$. Then, $\mathbf{Z} \overset{d}{=} \mathbf{U}\mathbf{Z}$ if and only if $\mathbf{Z}$ is a sub-Gaussian α-stable random vector with an underlying Gaussian vector having i.i.d. $\mathcal{N}(0,\sigma^2)$ components.*

Appendix C: Proof of Theorems 3 and 4

In this appendix, we prove Theorems 3 and 4. Both proofs follow a similar argument based on the following preliminaries.

Preliminaries

Let $N_1, N_2, \ldots$ be point processes with parameters $\kappa_1, \kappa_2, \ldots$ on $\mathbb{R}^2$ (for background point processes used in this appendix, see [58]). Then, the sequence $(N_n)_{n=1}^{\infty}$ converges in distribution to a point process N with parameter κ_∞ on $\mathbb{R}^2$; i.e., $N_n \overset{d}{\to} N$ if and only

if $\mathbb{E}[h(N_n)] \to \mathbb{E}[h(N)]$ for every bounded continuous function h on the space $\mathcal{N}$ of all counting measures on $\mathbb{R}^2$. Let $\mathcal{B}_N = \{B \in \mathcal{B} : N(\partial B) = 0\ a.s.\}$ and $\mathcal{C}_c^+$ be the set of all continuous functions $f : \mathbb{R}^2 \to \mathbb{R}_+$ with compact support. Convergence in distribution is characterized in the following theorem, which will provide the link between convergence in distribution of a point process and the convergence of the interference distribution it induces.

Theorem 6 (Theorem 6.1, [58]) *The following statements are equivalent*:

(i) $N_n \xrightarrow{d} N$.
(ii) $\int_{\mathbb{R}^2} f(x) N_n(\mathrm{d}x) \xrightarrow{d} \int_{\mathbb{R}^2} f(x) N(\mathrm{d}x)$ for all $f \in \mathcal{C}_c^+$.

In particular, consider the interference random vector in (5). *The real or imaginary component of the interference on a single subcarrier can be written in the form*

$$Z^{\kappa_n} = \sum_{j \in \Phi^{\kappa_n}_{\Gamma(r_{\min}, r_{\max})}} w_j \|\mathbf{x}_j\|^{-\eta/2}, \tag{35}$$

where $\Phi^{\kappa_n}_{\Gamma(r_{\min}, r_{\max})}$ *is the point process inducing the interference and* w_j *represents the real or imaginary part of a term* $h_{j,b_{u,i}} x_{j,b_{u,i}}$ *in* (4). *Under the hypotheses of Theorem* 3, *each* w_j *has compact support. Let* $f(\mathbf{x}, w) = w\|\mathbf{x}\|^{-\eta/2}$ *which is bounded and continuous since* $\Phi^{\kappa_n}_{\Gamma(r_{\min}, r_{\max})}$ *and each* w_j *lie in compact sets. As such, we immediately obtain convergence of distribution for* $\mathbf{Z}^{\kappa_n}$ *as* $n \to \infty$ *if (i) in Theorem* 6 *holds.*

To establish (i) in Theorem 6 holds, we require the following result.

Theorem 7 ([58, Theorem 6.2]) *Suppose N is simple and*

$$\lim_{m \to \infty} \limsup_{n \to \infty} P(N_n(B) > m) = 0,\ \forall\, B \in \mathcal{B}. \tag{36}$$

Then, $N_n \xrightarrow{d} N$ *if and only if*

$$\lim_{n \to \infty} P(N_n(B) = 0) = P(N(B) = 0),\ \forall\, B \in \mathcal{B}_N. \tag{37}$$

A sufficient condition for (37) *to hold is given by*

$$\limsup_{n \to \infty} \mathbb{E}[N_n(I)] \leq \mathbb{E}[N(I)] < \infty,\ \forall\, I \in \mathcal{I}_N, \tag{38}$$

where $\mathcal{I}_N$ *is the set of all intervals in* $\mathcal{B}_N$.

In order to apply Theorem 7, *we note that the point process inducing the interference in* (5) *can be viewed as an independently marked point process with points in* $\mathbb{R}^2$ *and marks in* $\mathbb{C}^{KN}$, *where KN is the total number of subcarriers. As* $\Phi^{\kappa_n}_{\Gamma(r_{\min}, r_{\max})}$ *is simple, the resulting marked process is simple as well.*

Proof of Theorem 3

We now establish that (38) holds, which will complete the proof. For the doubly Poisson cluster process, we have for all $I \in \mathcal{B}_{\Phi^{\kappa_n}_{\Gamma(r_{\min},r_{\max})}}$,

$$\mathbb{E}\left[\Phi^{\kappa_n}_{\Gamma(r_{\min},r_{\max})}(I)\right] = \mathbb{E}\left[\Phi^{\kappa_\infty}_{\Gamma(r_{\min},r_{\max})}(I)\right] + \mathbb{E}\left[\sum_{j\in\Phi^{\kappa_\infty}_{\Gamma(r_{\min},r_{\max})}} \Phi^{\kappa_n}_{d,j}(I)\right], \tag{39}$$

where κ_n denotes the density of daughter point process λ_d, where $\lim_{n\to\infty}\kappa_n = \kappa_\infty = 0$, and $\Phi^{\kappa_n}_{d,j}$ is the daughter point process corresponding to the j-th point in $\Phi^{\kappa_\infty}_{\Gamma(r_{\min},r_{\max})}$ which is the parent HPPP. Therefore by (38), we only need to show that

$$\limsup_{n\to\infty} \mathbb{E}\left[\sum_{j\in\Phi^{\kappa_\infty}_{\Gamma(r_{\min},r_{\max})}} \Phi^{\kappa_n}_{d,j}(I)\right] = 0. \tag{40}$$

Since each $\Phi^{\kappa_n}_{d,j}$ is a HPPP restricted to a particular region, it follows that the number of points in each I does not exceed that of the unrestricted HPPP. Since the expected number of points for a HPPP tends to zero as the intensity tends to zero, it follows that (40) holds.

Proof of Theorem 4

For the Matérn hard-core process of type II, (38) holds immediately since $\Phi^{\kappa_n}_{\Gamma(r_{\min},r_{\max})}$ is a thinned version of $\Phi^{\kappa_\infty}_{\Gamma(r_{\min},r_{\max})}$, where κ_n denotes the hard-core distance r_h and $\lim_{n\to\infty}\kappa_n = \kappa_\infty = 0$.

Appendix D: Derivation of (20)

In this appendix, we derive the approximation for the tail dependence and the correlation matrix in (20). To proceed, we first note that the tail dependence is not the same for each pair of elements in $\mathbf{Z}$. This is due to the fact that for a given msB B_u, the random vector is sub-Gaussian α-stable. This implies that for any pair of elements in $\mathbf{Z}_{B_u}$, the tail dependence is given by [45]

$$\lambda_{\mathbf{Z}_{B_u}} = \frac{\int_0^{\frac{1}{\sqrt{2}}} \frac{u^\alpha}{\sqrt{1-u^2}}\mathrm{d}u}{\int_0^1 \frac{u^\alpha}{\sqrt{1-u^2}}\mathrm{d}u}. \tag{41}$$

On the other hand, the tail dependence between pairs from different msBs in $\mathbf{Z}$ depends on the service rate p. For example, as $p \to 0$, elements of $\mathbf{Z}$ from different msBs are approximately independent. This means that the tail dependence for these pairs, denoted by $\lambda_{\tilde{\mathbf{Z}}}$, is approximately zero.

For $K > 1$, there are significantly more pairs of subcarriers with tail dependence $\lambda_{\tilde{\mathbf{Z}}}$ than $\lambda_{\mathbf{Z}_{B_u}}$. For this reason, we will base our estimate of the degree of freedom ν on $\lambda_{\tilde{\mathbf{Z}}}$ and verify that this approximation is accurate for sufficiently large p in Sect. 5.

The first step is then to obtain an approximation of the tail dependence $\lambda_{\tilde{\mathbf{Z}}}$. By definition,

$$\begin{aligned}\lambda_{\tilde{\mathbf{Z}}} &= \lim_{u\to 1} \Pr\left(\sum_{j\in\Phi_1} r_j^{-\frac{\eta}{2}} Z_{j,1} > F^{-1}(u) \middle| \sum_{j\in\Phi_2} r_j^{-\frac{\eta}{2}} Z_{j,2} > F^{-1}(u)\right), \\ &= \lim_{u\to 1} \frac{\Pr\left(\sum_{j\in\Phi_1} r_j^{-\frac{\eta}{2}} Z_{j,1} > F^{-1}(u) \middle| \sum_{j\in\Phi_2} r_j^{-\frac{\eta}{2}} Z_{j,2} > F^{-1}(u)\right)}{\Pr\left(\sum_{j\in\Phi_l} r_j^{-\frac{\eta}{2}} Z_{j,l} > x\right)}\end{aligned} \tag{42}$$

where $Z_{j,l} = \mathrm{Re}(h_{j,l}x_{j,l})$, $l = 1, \cdots, K$. By Property 1 in Appendix A and (10) in Theorem 1, for $l \in \{1, 2\}$, as $x \to \infty$

$$\begin{aligned}\Pr\left(\sum_{j\in\Phi_l} r_j^{-\frac{\eta}{2}} Z_{j,l} > x\right) &= \frac{1}{2} C_\alpha \gamma^\alpha x^{-\frac{4}{\eta}} + o\left(x^{-\frac{4}{\eta}}\right) \\ &= \frac{1}{2} p\lambda\pi \mathbb{E}[|Z_{1,1}||^\alpha] x^{-\frac{4}{\eta}} + o\left(x^{-\frac{4}{\eta}}\right).\end{aligned} \tag{43}$$

Moreover, the dependence is also strongest between elements of $\mathbf{Z}$ that have the same closest interferer distance, implied by Property 1. For $p \approx 1$, this suggests the approximation[6],

$$\begin{aligned}&\Pr\left(\sum_{j\in\Phi_1} r_j^{-\frac{\eta}{2}} Z_{j,1} > F^{-1}(u), \sum_{j\in\Phi_2} r_j^{-\frac{\eta}{2}} Z_{j,2} > F^{-1}(u)\right) \\ \approx & p\Pr\left(r_1^{-\frac{\eta}{2}} Z_{1,1} > F^{-1}(u), r_1^{-\frac{\eta}{2}} Z_{1,2} > F^{-1}(u)\right) \\ \approx & p\int_0^\infty \Pr\left(Z_{1,1} > F^{-1}(u) r^{\frac{\eta}{2}}, Z_{1,2} > F^{-1}(u) r^{\frac{\eta}{2}} | r\right) f_{r_1}(r) \mathrm{d}r.\end{aligned} \tag{44}$$

Since r_1 is the closest point in a HPPP, we have

$$f_{r_1}(r) = 2p\lambda\pi r e^{-p\lambda\pi r^2}. \tag{45}$$

This yields,

$$\begin{aligned}&\Pr\left(\sum_{j\in\Phi_1} r_j^{-\frac{\eta}{2}} Z_{j,1} > F^{-1}(u), \sum_{j\in\Phi_2} r_j^{-\frac{\eta}{2}} Z_{j,2} > F^{-1}(u)\right) \\ \approx & p\int_0^\infty \left(1 - F_{Z_{1,1}}\left(F^{-1}(u) r^{\frac{\eta}{2}}\right)\right)^2 2p\lambda\pi r e^{-p\lambda\pi r^2} \mathrm{d}r.\end{aligned} \tag{46}$$

Applying the change of variables, $z = F^{-1}(u) r^{\frac{\eta}{2}}$ and combining with (42) and (43), then yields (20).

To derive an estimate of Σ, we recall that for $p = 1$, the interference random vector $\mathbf{Z}$ approximately forms an isotropic sub-Gaussian α-stable random vector (by Theorem 2). In this case, Σ is the identity matrix as the underlying Gaussian random vector is

[6] When the interference forms a real vector, this argument can be made rigorous [59].

isotropic. To obtain an approximation of Σ for $p \approx 1$, we therefore base our estimate on the case $p = 1$.

Abbreviations
IoT: Internet of things; NB-IoT: Narrowband internet of things; HPPP: Homogeneous Poisson point process; MRC: Maximum ratio combining; CSMA: Channel sense multiple access; NPUSCH: Narrowband physical uplink shared channel; SCMA: Sparse code multiple access; KL divergence: Kullback–Leibler divergence; OFDM: Orthogonal frequency division multiplexing; LPWAN: Low power wide area networks; msB: Minimum size block.

Authors' contributions
CZ, ME, LC, GWP and JG all contributed to formulation of the research problem, mathematical analysis, numerical simulations, and writing of the paper. All authors read and approved the final manuscript.

Funding
This work has been (partly) funded by the French National Agency for Research (ANR) under grant ANR-16-CE25-0001 - ARBURST. It has also been supported by IRCICA, USR CNRS 3380, Lille, France and the COST Action CA15104 IRACON.

Availability of data and materials
N/A.

Declarations

Competing interests
The authors declare that they have no competing interests.

Ethics approval and consent to participate
N/A.

Consent for publication
N/A.

Author details
[1]University of Lille, Lille, France. [2]CITI Laboratory, Univ Lyon, INSA Lyon, Inria, Villeurbanne, France. [3]School of Mathematical and Computer Sciences, Heriot-Watt University, Edinburgh, UK.

Received: 15 March 2021 Accepted: 10 March 2022
Published online: 28 March 2022

References

1. J.G. Andrews, F. Baccelli, R.K. Ganti, A tractable approach to coverage and rate in cellular networks. IEEE Trans. Commun. **59**(11), 3122–3134 (2011)
2. H. ElSawy, E. Hossain, M. Haenggi, Stochastic geometry for modeling, analysis, and design of multi-tier and cognitive cellular wireless networks: a survey. IEEE Commun. Surv. Tutor. **15**(3), 996–1019 (2013)
3. T. Bai, R.W. Heath, Analyzing uplink SINR and rate in massive MIMO systems using stochastic geometry. IEEE Trans. Commun. **64**(11), 4592–4606 (2016)
4. H. ElSawy, A. Sultan-Salem, M.S. Alouini, M.Z. Win, Modeling and analysis of cellular networks using stochastic geometry: a tutorial. IEEE Commun. Surv. Tutor. **19**(1), 167–203 (2017)
5. M. Haenggi, R.K. Ganti, Interference in large wireless networks. Found. Trends Netw. **3**(2), 127–248 (2009)
6. K. Gulati, B.L. Evans, J.G. Andrews, K.R. Tinsley, Statistics of co-channel interference in a field of Poisson–Poisson clustered interferers. IEEE Trans. Signal Process. **58**(12), 6207–6222 (2010)
7. F. Baccelli, B. Blaszczyszyn, P. Muhlethaler, An aloha protocol for multihop mobile wireless networks. IEEE Trans. Inf. Theory **52**(2), 421–436 (2006)
8. M. Di Renzo, S. Wang, X. Xi, Inhomogeneous double thinning—modeling and analysis of cellular networks by using inhomogeneous Poisson point processes. IEEE Trans. Wirel. Commun. **17**(8), 5162–5182 (2018)
9. N. Deng, W. Zhou, M. Haenggi, The Ginibre point process as a model for wireless networks with repulsion. IEEE Trans. Wirel. Commun. **14**(1), 107–121 (2015)
10. 3GPP TR 21.915 version 15.0.0 Release 15. https://www.etsi.org/deliver/etsi_tr/121900_121999/121915/15.00.00_60/tr_121915v150000p.pdf
11. A. Hoglund et al., Overview of 3GPP release 14 enhanced NB-IoT. IEEE Netw. **31**(6), 16–22 (2017)
12. H. Nikopour, H. Baligh, Sparse code multiple access, in: IEEE International Symposium on Personal Indoor and Mobile Radio Communications (PIMRC) (2013)
13. E.S. Sousa, Performance of a spread spectrum packet radio network link in a Poisson field of interferers. IEEE Trans. Inf. Theory **38**(6), 1743–1754 (1992)
14. J. Ilow, D. Hatzinakos, Analytic alpha-stable noise modeling in a Poisson field of interfers or scatterers. IEEE Trans. Signal Process. **46**(6), 1601–1611 (1998)
15. P.C. Pinto, M.Z. Win, Communication in a Poisson field of interferers-part I: interference distribution and error probability. IEEE Trans. Wirel. Commun. **9**(7), 2176–2186 (2010)

16. P.C. Pinto, M.Z. Win, Communication in a Poisson field of interferers-part II: channel capacity and interference spectrum. IEEE Trans. Wirel. Commun. **9**(7), 2187–2195 (2010)
17. M. Lauridsen, B. Vejlgaard, I. Kovács, H.C. Nguyen, P.E. Mogensen, Interference measurements in the European 868 MHz ISM band with focus on LoRa and SigFox, in IEEE Wireless Communications and Networking Conference (WCNC) (2017)
18. B. Vejlgaard, M. Lauridsen, H. Nguyen, I.Z. Kovács, P. Mogensen, M. Sorensen, Interference impact on coverage and capacity for low power wide area IoT networks, in 2017 IEEE Wireless Communications and Networking Conference (WCNC) (IEEE, 2017), p. 1–6
19. L. Clavier, T. Pedersen, I. Rodriguez, M. Lauridsen, M. Egan, Experimental evidence for heavy tailed interference in the IoT. IEEE Commun. Lett. **25**(3), 692–695 (2021)
20. S. Niranjayan, N.C. Beaulieu, The BER optimal linear rake receiver for signal detection in symmetric alpha-stable noise. IEEE Trans. Commun. **57**(12), 3585–3588 (2009)
21. S. Niranjayan, N.C. Beaulieu, BER optimal linear combiner for signal detection in symmetric alpha-stable noise: small values of alpha. IEEE Trans. Wirel. Commun. **9**(3), 886–890 (2010)
22. G. Wu, L. Clavier, Decoding metric study for turbo codes in very impulsive environment. IEEE Commun. Lett. **16**(2), 256–258 (2011)
23. J. Riihijarvi, P. Mahonen, Modeling spatial structure of wireless communication networks, in IEEE Conference on Computer Communications Workshops (2010)
24. B. Cho, K. Koufos, R. Jantti, Bounding the mean interference in Matérn type II hard-core wireless networks. IEEE Wirel. Commun. Lett. **2**(5), 563–566 (2013)
25. M. Haenggi, Mean interference in hard-core wireless networks. IEEE Commun. Lett. **15**(8), 792–794 (2011)
26. U. Schiler, J. Schmidt, C. Bettstetter, On interference dynamics in Matérn networks. IEEE Trans. Mob. Comput. **19**(7), 1677–1688 (2020)
27. X. Yang, A.P. Petropulu, Co-channel interference modeling and analysis in a Poisson field of interferers in wireless communications. IEEE Trans. Signal Process. **51**(1), 64–76 (2003)
28. M. Freitas, M. Egan, L. Clavier, A. Savard, J.-M. Gorce, Power control in parallel symmetric α-stable noise channels, in IEEE International Workshop on Signal Processing Advances in Wireless Communications (2018)
29. M. de Freitas, M. Egan, L. Clavier, G.W. Peters, N. Azzaoui, Capacity bounds for additive symmetric alpha-stable noise channels. IEEE Trans. Inf. Theory **63**(8), 5115–5123 (2017)
30. J. Fahs, I. Abou-Faycal, On properties of the support of capacity-achieving distributions for additive noise channel models with input cost constraints. IEEE Trans. Inf. Theory **64**(2), 1178–1198 (2018)
31. R. Nelson, *An Introduction to Copulas* (Springer, New York, 1999)
32. J. Kitchen, W. Moran, Copula techniques in wireless communications. ANZIAM J. **51**, 526–540 (2010)
33. M.H. Gholizadeh, H. Amindavar, J.A. Ritcey, On the capacity of MIMO correlated Nakagami-m fading channels using copula. EURASIP J. Wirel. Commun. Netw. **1**, 1–11 (2015)
34. X. Yan, L. Clavier, G.W. Peters, N. Azzaoui, F. Septier, I. Nevat, Skew-t copula for dependence modelling of impulsive (alpha-stable) interference, in IEEE International Conference on Communications (ICC) (2015)
35. E. Soret, L. Clavier, G.W. Peters, I. Nevat, SIMO communication with impulsive and dependent interference—the Copula receiver, in Actes du XXVIème Colloque GRETSI (2017)
36. C. Zheng, M. Egan, L. Clavier, G.W. Peters, J.-M. Gorce, Copula-based interference models for iot wireless networks, in ICC 2019-2019 IEEE International Conference on Communications (ICC) (IEEE, 2019), p. 1–6
37. M. Haenggi, *Stochastic Geometry for Wireless Networks* (Cambridge University Press, New York, 2013)
38. Y. Zhong, G. Mao, X. Ge, F.-C. Zheng, Spatio-temporal modeling for massive and sporadic access. IEEE J. Select. Areas Commun. **39**(3), 638–651 (2021)
39. A. Mahmood, M. Chitre, M.A. Armand, PSK communication with passband additive symmetric α-stable noise. IEEE Trans. Commun. **60**(10), 2990–3000 (2012)
40. M. Egan, L. Clavier, C. Zheng, M. de Freitas, J.-M. Gorce, Dynamic interference for uplink SCMA in large-scale wireless networks without coordination. EURASIP J. Wirel. Commun. Netw. **1**, 1–14 (2018)
41. H.-B. Fang, K.-T. Fang, S. Kotz, The meta-elliptical distributions with given marginals. J. Multivar. Anal. **82**(1), 1–16 (2002)
42. A.A. Balkema, P. Embrechts, N. Nolde, Meta densities and the shape of their sample clouds. J. Multivar. Anal. **101**(7), 1738–1754 (2010)
43. J.P. Nolan, Multivariate elliptically contoured stable distributions: theory and estimation. Comput. Stat. **28**(5), 2067–2089 (2013)
44. P. Billingsley, *Convergence of Probability Measures* (Wiley, New York, 1999)
45. S. Demarta, A.J. McNeil, The *t*-copula and related copulas. Int. Stat. Rev. **73**(1), 111–129 (2005)
46. H. Joe, J. Xu, The estimation method of inference functions for margins for multivariate models. Technical Report 166, Department of Statistics, University of British Columbia (1996)
47. M. Cruz, G.W. Peters, P.V. Shevchenko, *Fundamental Aspects of Operational Risk and Insurance Analytics: A Handbook of Operational Risk* (Wiley, Hoboken, 2015)
48. F. Lindskog, A. Mcneil, U. Schmock, Kendall's tau for elliptical distributions, in Credit Risk (Physica-Verlag HD, Heidelberg, 2003), p. 149–156
49. P. Rousseeuw, G. Molenberghs, Transformation of non positive definite semidefinite correlation matrices. Commun. Stat. Theory Methods **22**, 965–984 (1993)
50. J.H. McCulloch, Simple consistent estimators of stable distribution parameters. Commun. Stat. Simul. Comput. **15**(4), 1109–1136 (1986)
51. M. Veillette, Alpha-Stable distributions in MATLAB. http://math.bu.edu/people/mveillet/html/alphastablepub.html
52. Z. Szabó, Information theoretical estimators toolbox. J. Mach. Learn. Res. **15**, 283–287 (2014)
53. Q. Wang, S.R. Kulkarni, S. Verdú, A nearest-neighbor approach to estimating divergence between continuous random vectors, in 2006 IEEE International Symposium on Information Theory (IEEE, 2006), p. 242–246

54. A.M. Ibrahim, T. ElBatt, A. El-Keyi, Coverage probability analysis for wireless networks using repulsive point processes, in 2013 IEEE 24th Annual International Symposium on Personal, Indoor, and Mobile Radio Communications (PIMRC) (IEEE, 2013), p. 1002–1007
55. C. Zheng, M. Egan, T. Pedersen, J.-M. Gorce, Linear combining in dependent α-stable interference, in Proceedings of IEEE International Conference on Communications (ICC) (2020)
56. C.L. Nikias, M. Shao, *Signal Processing with Alpha-stable Distributions and Applications* (Wiley, New York, 1995)
57. G. Samorodnitsky, M.S. Taqqu, *Stable Non-Gaussian Random Processes* (CRC Press, New York, 1994)
58. R.F. Serfozo, Point processes, in *Handbooks in Operations Research and Management Science*, vol. 2, 1st edn., ed. by D.P. Heyman, M.J. Sobel (Elsevier Science Publishers B.V., North-Holland, 1990), pp. 1–93
59. M. Egan, Dependence testing via extremes for regularly varying models, in IEEE International Symposium on Information Theory (ISIT) (2021)

Publisher's Note